International Journal of Microwave and Wireless Technologies

cambridge.org/mrf

RCS prediction and optimization for anomalous reflection metasurfaces using Floquet analysis

Matthieu Elineau[1,2], Renaud Loison[1], Stéphane Méric[1], Raphaël Gillard[1], Pascal Pagani[2], Geneviève Mazé-Merceur[2] and Philippe Pouliguen[3]

[1]IETR, INSA Rennes, UMR 6164, Rennes, France; [2]CEA, DAM, CESTA, Le Barp, France and [3]DGA, AID, Paris, France

Research Paper

Cite this article: Elineau M, Loison R, Méric S, Gillard R, Pagani P, Mazé-Merceur G, Pouliguen P (2023). RCS prediction and optimization for anomalous reflection metasurfaces using Floquet analysis. *International Journal of Microwave and Wireless Technologies* **15**, 966–974. https://doi.org/10.1017/S1759078722001398

Received: 29 July 2022
Revised: 9 November 2022
Accepted: 10 November 2022

Author for correspondence:
Matthieu Elineau,
E-mail: matthieu.elineau.scholar@gmail.com

Abstract

Due to their periodic nature, metasurfaces used to perform anomalous reflection raise parasitic harmonic reflections. We show a classical synthesis example of such a structure and highlight its limitations. Floquet analysis and its associated simulation environment are exploited to understand the origin of these parasitic reflections and to mitigate them. The proposed method is based on the optimization of the metasurface periodic pattern: the supercell. A predictive method is built to calculate radar cross-section patterns from supercell Floquet simulation, avoiding dealing with heavy simulations. The proposed model, the optimization outputs, and the general results are exposed in details. Different cases are also discussed to prove the repeatability of the proposed method. An earlier version of this paper was presented at the European Microwave Conference and was published in its proceedings.

Introduction

Metasurfaces [1, 2] have made possible a great quantity of electromagnetic wavefront manipulation types over the last decade [3]. In the field of radar, they spread their capabilities over various applications such as camouflaging techniques or radar cross-section (RCS) reduction [4, 5], backscattering enhancement [6], or anomalous reflection [7, 8].

Historically, a very simple optical physics principle gave rise to phase gradient metasurfaces [9]. The introduced generalized Snell's law allowed the design of anomalous reflectors of great simplicity, regarding either the underlying physics or the realization process. However, the inherent translation invariances of these structures raise spurious diffraction modes, which forced the community to find a more elaborated physical framework by incorporating Floquet theory to it. Periodic structures are very common in various physical domains, such as condensed matter physics where the Floquet–Bloch theory is already a very usual tool [10]. Applied to electromagnetic control, several research domains have emerged such as glide symmetric structures [11], or metagratings [12, 13] where the objective is to channel the power from one Floquet mode into an other.

In the domain of anomalous reflection metasurfaces, it has been shown that it is difficult or even impossible to produce efficient passive reflective surfaces without considering non-local designs or polarization conversions [14, 15].

In this context, we propose an efficient optimization approach to shape the bistatic RCS of anomalous reflection metasurfaces. It relies on the method presented in [16] which merges gradient metasurface approach and Floquet analysis. We build a fast predictive tool and use it in an optimization routine to design anomalous reflection metasurfaces with mitigated spurious diffraction modes.

The paper is organized as follows: section "Classical synthesis and its limitations" discusses the classical synthesis procedure and its limitations that are overcome by the use of Floquet analysis as presented in section "Floquet analysis." An optimization process, taking advantage of the introduced considerations, is described in section "Metasurface optimization." The application of the method is discussed and illustrated through specific study cases presented in section "Further examples."

Classical synthesis and its limitations

Anomalous reflection configuration

The chosen anomalous reflection configuration is the one depicted in Fig. 1.

A plane wave coming from the direction θ_i impinges on a surface lying in a *Oxy* plane and is converted into an other plane wave reflected in the direction θ_r. Both waves are transverse magnetic polarized (TM, $\boldsymbol{H}\perp Oyz$). The anomalous reflection is made possible by the presence of a linearly varying reflection phase distribution along $\boldsymbol{u}_y$ at the reflecting surface [9].

© The Author(s), 2023. Published by Cambridge University Press in association with the European Microwave Association. This is an Open Access article, distributed under the terms of the Creative Commons Attribution licence (http://creativecommons.org/licenses/by/4.0/), which permits unrestricted re-use, distribution and reproduction, provided the original article is properly cited.

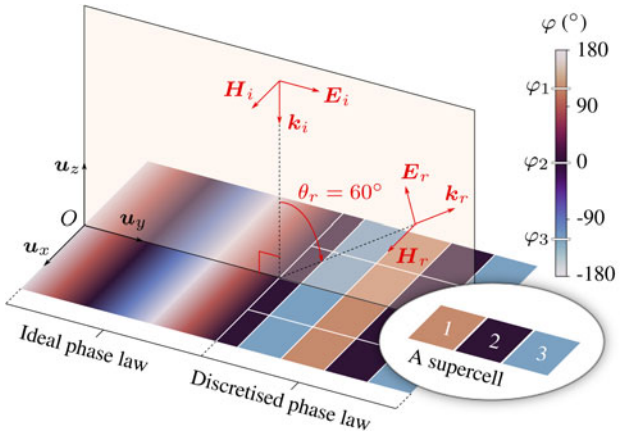


Fig. 1. Anomalous reflection of a TM plane wave occurring in the *Oyz* plane, with an ideal or a discretized linear phase gradient lying in the *Oxy* plane.

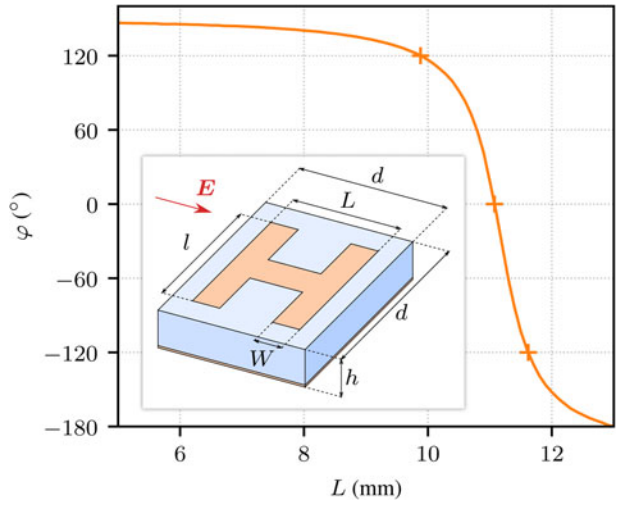


Fig. 2. Variation of the phase response of the H cell versus L in infinite periodic environment for $l = 3$ mm. Fixed parameters are $h = 1.6$ mm, $d = 14.43$ mm, and $W = 2$ mm.

A solution to synthesize such a phase gradient is to discretize it by using reflective cells. The discretization choice here is such that each gradient spatial period D_y is covered with a same periodically distributed supercell, composed itself of three cells of size d. The phase law can be written in three equivalent ways to express the useful dimensions:

$$\sin(\theta_r) - \sin(\theta_i) = \frac{1}{k}\frac{\mathrm{d}\varphi}{\mathrm{d}y} = \frac{1}{k}\frac{2\pi}{D_y} = \frac{\lambda}{3d} \tag{1}$$

where k and λ are the wave number and wavelength at a given frequency f, θ_i the direction of the incoming plane wave, and θ_r the direction of the reflected one. For $f = 8$ GHz, $\theta_i = 0°$, and the anomalous reflection angle being set, for our example, to $\theta_r = 60°$, the two other dimensions are deduced: $D_y \approx 43.3$ mm and $d \approx 14.43$ mm.

Phase law synthesis

To produce the desired phase law, H shape patch cells studied in [17] are used. The cells consist of a perfect electric conductor (PEC) patch on top of a dielectric substrate of relative permittivity $\epsilon_r = 2.17$, backed by a PEC plane. Figure 2 presents the geometrical parameters of the cells as well as a phase response as a function of one parameter: the patch length L.

Table 1. Geometrical parameters of the initial supercell

p	l_p (mm)	L_p (mm)	φ_p (°)
1	3	9.881	120
2	3	11.075	0
3	3	11.619	−120

The three cells constituting the supercell must produce regularly spaced phase responses to create the linear phase variation. The needed geometrical parameters for each cell $p \in \{1, 2, 3\}$, highlighted on the trace of Fig. 2 by crosses, are listed in Table 1, as well as their phase response.

The supercell is then replicated nine times in the $\boldsymbol{u}_y$ direction to produce an approximate array length of 10 λ. The array is studied in full-wave simulation using HFSS with absorbing boundary conditions along $\boldsymbol{u}_y$ and a perfect magnetic conductor along $\boldsymbol{u}_x$ to ensure infinite periodicity along the $\boldsymbol{u}_x$ direction of TM polarization. The radiated fields are used to calculate a bistatic RCS pattern [18] that is shown in Fig. 3 in solid line.

The structure mainly radiates in the desired direction $\theta = 60°$, but also shows noticeable radiation levels in two other main directions : $\theta = 0°$ and $\theta = -60°$.

Limitations of the approach

During the synthesis procedure the surface is considered as an array of cells only characterized by their reflection coefficients $\Gamma_p = e^{j\varphi_p}$, in such a way they are hosting a source field

$$\boldsymbol{E}_{s,p} = E_0 \boldsymbol{u}_y \Gamma_p = E_0 \boldsymbol{u}_y e^{j\varphi_p} \tag{2}$$

E_0 being a unitary amplitude and φ_p taking only the three possible values presented in subsection "Phase law synthesis" with $\varphi_p = \varphi_{p+3}$. This source field can be converted into current densities and used in radiating integrals [19] to calculate the field created by a vacuum-surrounded aperture hosting this source field. The obtained field is summed over all the 27 contributing cells to obtain a bistatic RCS diagram that is compared to the simulated one in Fig. 3.

This basic synthesis approach does not take into account the two parasitic radiation directions as only the main lobe at $\theta_r = 60°$ is predicted by the analytical model. It is worth mentioning that, despite the simplicity of this approach, the main lobe level is well estimated by the analytical model, with only 0.4 dB difference with respect to the full-wave HFSS simulation.

Floquet analysis

Expected behavior

The periodicity of the array, obtained by the replication of the supercell, is the cause of the parasitic reflections. To understand this phenomenon, we study the structure with the help of Floquet analysis. The total three main radiation directions are predicted by Floquet analysis [20]. They correspond to every m that

https://doi.org/10.1017/S1759078722001398 Published online by Cambridge University Press

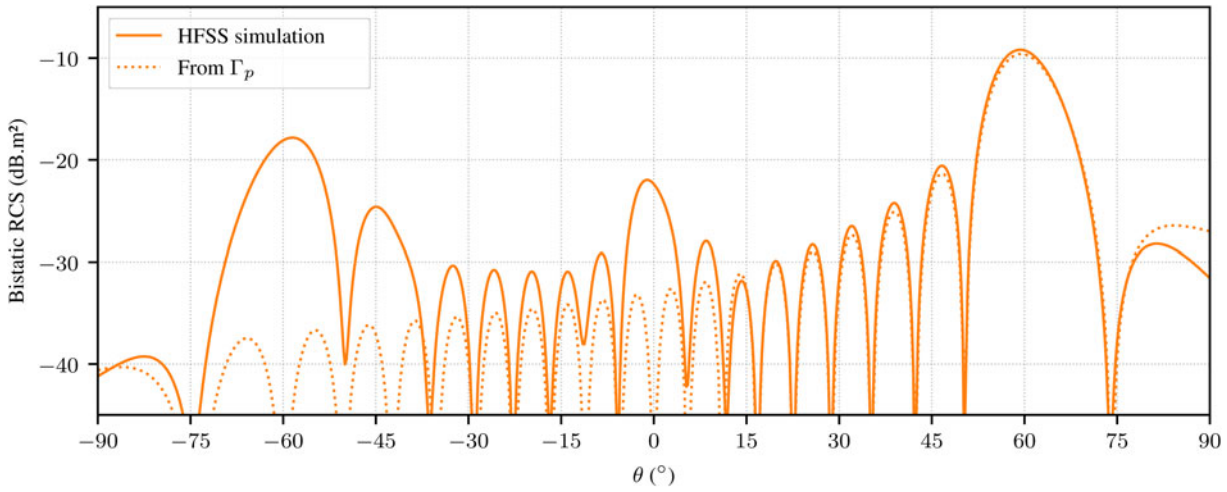


Fig. 3. Bistatic RCS for $\theta_i = 0°$ of the initial surface compared to the analytical one used to design the surface.

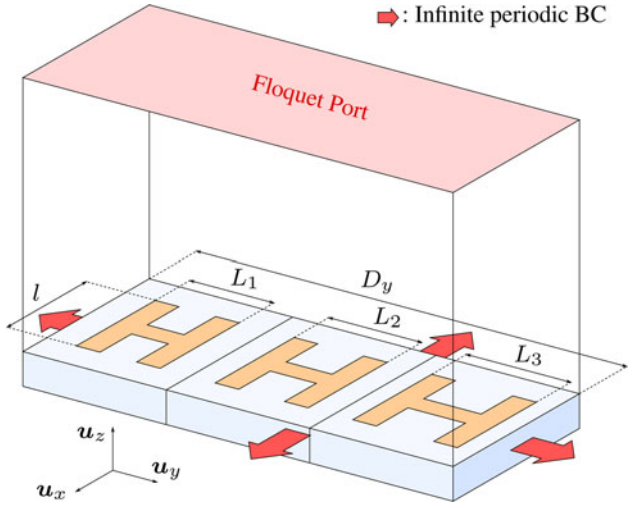


Fig. 4. The supercell in Floquet-type simulation.

provides real solutions to the equation

$$k_{zm}^2 = k^2 - k_{ym}^2 \tag{3}$$

where

$$k_{ym} = k_{y0} + \frac{2m\pi}{D_y} \tag{4}$$

with k_{y0} and k_{ym} the components along $\boldsymbol{u}_y$ of the $\boldsymbol{k}_0$ and $\boldsymbol{k}_m$ wave vectors respectively. The first one is associated to the fundamental Floquet mode and the second one is associated to one harmonic Floquet mode. In the considered case, as the incoming and reflected waves propagate in the same medium, $\boldsymbol{k}_0 = \boldsymbol{k}_m = k$. Writing down $k_{y0} = k\sin(\theta_0)$ and $k_{ym} = k\sin(\theta_m)$ in (4) leads to

$$\sin(\theta_m) - \sin(\theta_0) = \frac{1}{k}\frac{2\pi}{D_y} \tag{5}$$

which is the generalized reflection law, written in (1), where θ_m is the intended reflection direction after an illumination in the θ_0 direction. Performing anomalous reflection, with the help of the generalized reflection law, while setting the structure periodicity equal to the gradient periodicity is strictly equivalent to satisfy the $m = 1$ Floquet mode propagation condition. We also verify that in our case the modes $m = -1$ and $m = 0$ are propagative and correspond to the directions of the parasitic radiations observed in the previous section.

Table 2. $S_{m,0}$ parameters of the initial supercell

m	$S_{m,0}$	$\lvert S_{m,0}\rvert$ (dB)
−1	$0.265 - 0.221j$	−9.24
0	$-0.058 - 0.140j$	−16.41
1	$0.874 + 0.264j$	−0.79

Usage of the Floquet-type simulation

In the light of the previous analysis, the anomalous reflection structure can be seen as a reflecting surface that has a conversion capability between the different propagative modes. To understand its behavior, the supercell can be simulated in a Floquet environment, as depicted in Fig. 4.

The supercell is infinitely replicated by the mean of master/slave pairs defined along the $\boldsymbol{u}_x$ and $\boldsymbol{u}_y$ directions. This allows to define a Floquet port that can be used to excite the structure.

Simulating such a structure gives access to a multimode coupling matrix whose elements are the $S_{m,n}$ complex parameters defined as

$$E_m = S_{m,n}E_n \tag{6}$$

where E_m is the complex field amplitude in a *m reflected* mode while the structure is studied under a *n exciting* mode of field amplitude E_n. The parameters of interest in our example are the $S_{m,0}$ because they correspond to an excitation with the $n = 0$ mode, which corresponds to an incidence of $\theta = 0°$.

The $S_{m,0}$ parameters of the simulated supercell used to create the initial array are reported in Table 2. The $S_{-1,0}$ parameter is

https://doi.org/10.1017/S1759078722001398 Published online by Cambridge University Press

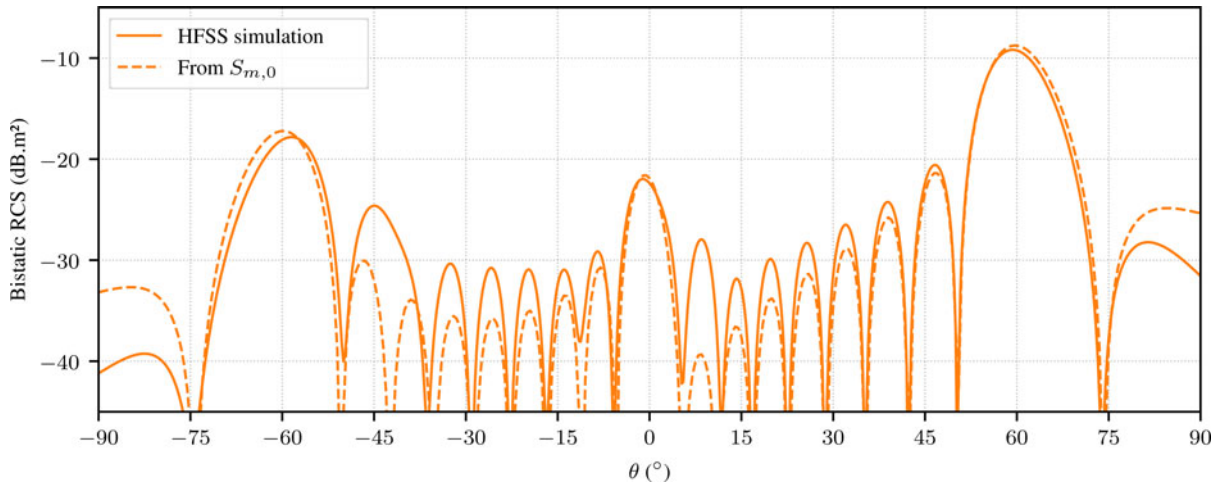


Fig. 5. Bistatic RCS for $\theta_i = 0°$ of the initial surface compared to the analytical one using $S_{m,0}$ simulation parameters.

Table 3. $S_{m,0}$ parameters of the optimized supercell

m	$S_{m,0}$	$\lvert S_{m,0}\rvert$ (dB)
−1	$-0.153 - 0.050j$	−15.89
0	$-0.084 - 0.085j$	−18.45
1	$0.685 - 0.683j$	−0.29

Table 4. Geometrical parameters of the optimized supercell

p	l_p (mm)	L_p (mm)	φ_p (°)
1	4.418	9.372	66.3
2	3.224	11.119	−73.86
3	3.132	12.189	−165.26

highlighted as it will be useful to be compared in the coming study of section "Metasurface optimization."

It can already be noticed that the weights in decibels attributed to each mode roughly follow the same hierarchy than the corresponding lobe levels observed on the RCS diagram.

Incorporation of $S_{m,0}$ parameters in the model

As described in subsection "Limitations of the approach," a radiated field can be obtained considering source fields on the surface. This time, the surface is not seen as an array of cells any more, but in its entirety, hosting three different source fields for the three possible values of m

$$\boldsymbol{E}_{s,m} = E_0 \boldsymbol{u}_y S_{m,0} e^{-jk \sin(\theta_m) y} \tag{7}$$

Each source field is of unitary amplitude E_0 with a weighting $S_{m,0}$, obtained from Table 2, and a phase variation corresponding to the considered Floquet mode. Source fields are again converted into current densities and used in radiation integrals. The three radiated fields are summed and give the bistatic RCS shown in Fig. 5 in dashed line.

The new source fields correctly reproduce the behavior of the simulated surface. Each main lobe level is well predicted, while the nine-supercell array is finite along $\boldsymbol{u}_y$, in contrast with Floquet-type simulation. This conclusion gives credit toward a representation of the surface with using only the S parameters associated to the supercell, thus avoiding the burdensome simulation type required to solve the whole structure. Taking advantage of this situation, we propose to perform S parameter optimizations, obtained with effortless simulations, that are expected to have a quantitative repercussion on the bistatic RCS of the complete structure.

Metasurface optimization

Process

The geometrical parameters of the cells (l_p, L_p) are chosen to be the optimization input variables and the objective is to minimize the level of the $S_{-1,0}$ parameter. This definition is arbitrary and suits a particular application, the method is not restricted to it and can be used for other specifications. One may want to work for example with any $S_{-n,n}$ parameter, corresponding to backscattering that is of specific interest for numerous RCS applications. Indices m and n can also be larger than 1, if the supercell length is set accordingly. Our proposed approach can theoretically be extended to the optimization of such supercells with more higher-order Floquet modes. The formalism using S parameters remains basically the same and so does the power-transfer mechanism between propagative modes. Of course, the optimization problem gets more complex and more degrees of freedom might be needed to solve it. The cost function to be minimized is then

$$f_c(l_p, L_p) = -(|S_{1,0}| - |S_{-1,0}|) \tag{8}$$

The aim is then to increase the difference between the lobe levels associated to the modes $m = -1$ and $m = 1$, avoiding the solutions where both of them are low, and without having a particular interest in handling the mode $m = 0$.

Starting a gradient type optimization process from the first supercell dimensions as an initial guess, the solution is expected to be close to the initial one, as it is already shaped from the phase gradient. In the same spirit, the cells used in the array are obviously in a different environment than the infinite periodic one used to obtain their phase response. The proposed optimization

https://doi.org/10.1017/S1759078722001398 Published online by Cambridge University Press

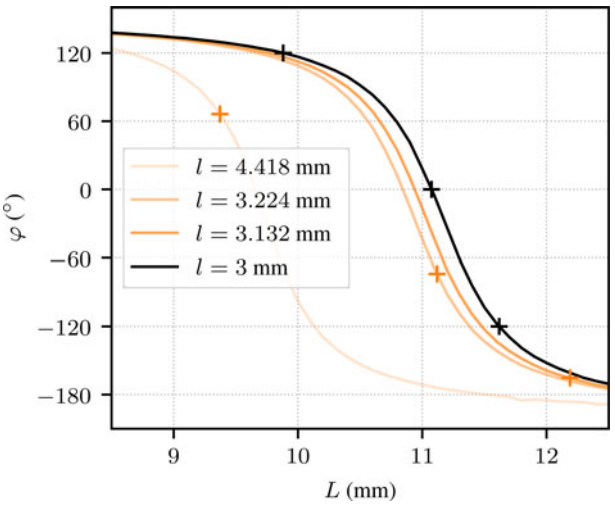


Fig. 6. Evolution of phase responses of the cells after an optimization process. The three new phase variations with L are computed the same way than the already presented one (in black), each one for the three optimized values of l.

process can thus be seen as a way to better take into account the neighborhood of each cell, as the whole supercell is simulated.

Finally, based on our observations, we experience that some parameters are more sensitive than others. For example, as the L dimension is oriented along $\boldsymbol{E}$, it shows a greater influence on S parameters than l. Hence, the critical dimension L can be first used in a rough analysis and l can be used afterwards for a fine tuning. A similar reasoning process can be applied to deal with sensitive cells, that are close to resonance, before others.

Results

Carrying the optimization process previously described leads to optimized S parameters presented in Table 3 and associated to the optimized dimensions presented in Table 4. New phase responses can be obtained by simulating the optimized cells (constituing the optimized supercell) in an infinite periodic environment, they are also presented in Table 4.

The $|S_{-1,0}|$ level drops by a significant amount, while the two others are maintained. This already announces a more efficient

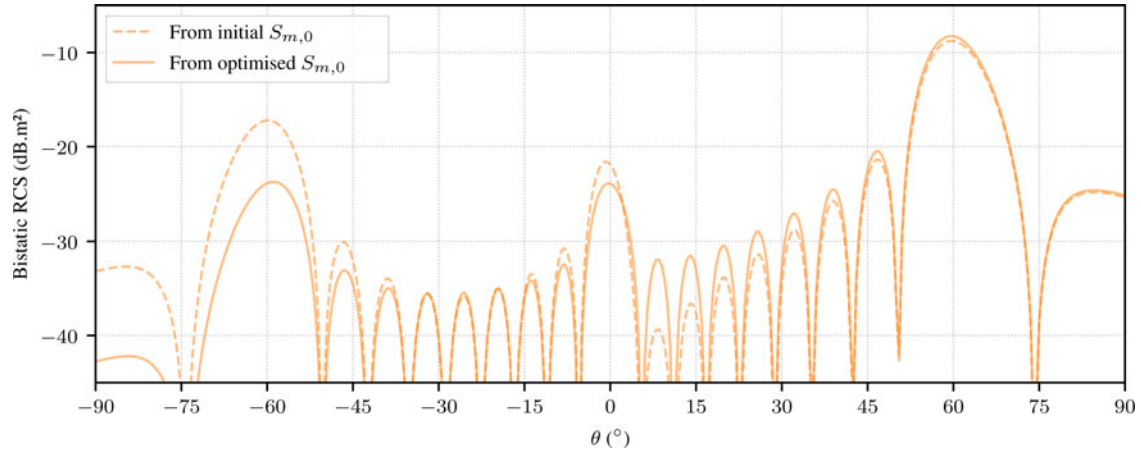


Fig. 7. Bistatic RCS for $\theta_i = 0°$ of the optimized surface compared to the one of the initial surface. Both of them are obtained using their $S_{m,0}$ associated simulation parameters.

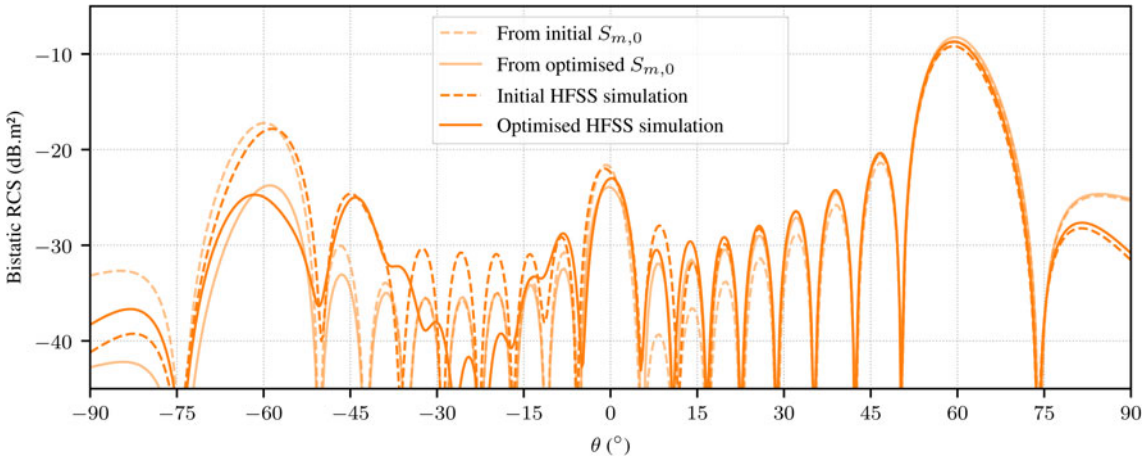


Fig. 8. Bistatic RCS for $\theta_i = 0°$ of the optimized surface compared to the one of the initial surface, in rigorous simulation and by using S parameters.

https://doi.org/10.1017/S1759078722001398 Published online by Cambridge University Press

Table 5. Evolution of the supercell dimensions during the optimization process

p	l_p (mm)	L_p (mm)	φ_p (°)
Initial supercell			
1	8	6.43	120
2	8	7.04	0
3	8	7.30	−120
Optimized supercell			
1	8.313	6.342	116.80
2	7.978	7.083	−17.94
3	7.999	7.258	−105.42

Case $l = 8$ mm.

Table 6. Evolution of the supercell $S_{m,0}$ parameters during the optimization process

m	$S_{m,0}$	$\lvert S_{m,0}\rvert$ (dB)
Initial supercell		
−1	$-0.070 - 0.132j$	−16.52
0	$-0.026 + 0.019j$	−29.81
1	$0.970 - 0.004j$	−0.26
Optimized supercell		
−1	$0.009 + 0.001j$	−40.50
0	$0.065 - 0.136j$	−16.42
1	$0.967 - 0.047j$	−0.28

Case $l = 8$ mm.

mode conversion capability of the surface, for our specific application. It can also be seen that the new phase responses drifts out from the resonance region, where it is expected that they are more stable once in an array. This phenomena is illustrated in Fig. 6 where it can be seen that new phase responses now escape the $\varphi = 0°$ region where the slope is greater. These geometrical variations are also very small, barely more than half a millimeter in most cases. This observation brings more confidence in the choice of the initial simple phase gradient, so it only needs a small adjustment to perform well.

New $\boldsymbol{E}_{s,m}$ can now be computed using the optimized $S_{m,0}$ parameters and then be used to calculate the expected RCS of the optimized array. This RCS is plotted in Fig. 7 where the initial calculated RCS is reminded.

It must still be verified that the new array has the expected behavior with a rigorous simulation. The optimized geometry is put in the same full-wave environment than the initial one so they can be compared. Figure 8 shows the performances of the initial and optimized array as well as their predicted behavior by the use of S parameters. The global comparison is a way to check that the method is predictive as expected.

Indeed, the model correctly predicts both the initial and optimized structure behaviors. A 7.5 dB decrease of the parasitic lobe level is obtained while maintaining other radiation directions at a similar level.

Further examples

This section presents the optimization results of two others anomalously reflecting surface, where the initial l values are chosen to be 8 and 12 millimeters.

Case of l = 8 *mm*

Since the complete procedure has already been discussed, we propose here to only give concluding results and to comment them. Tables 5 and 6 give the geometrical variations and $S_{m,0}$ parameter evolutions through the optimization process. Figure 9 shows the global bistatic RCS comparisons.

The $|S_{-1,0}|$ level drastically decreases, but one should carefully keep in mind that the initial level was lower compared to the previous case. In contrast, the $|S_{0,0}|$ level raises as the optimization process does not handle it. Geometrical variations of the supercell are smaller than in the first $l = 3$ mm case and so it is for phase response evolution. The largest geometrical variation for this case is 4% of the initial cell size and is in contrast about 32% for the first presented case. The optimized array performance is greatly improved, by an attenuation of 15 dB on the parasitic lobe level. Nevertheless, the model is less quantitative in this region where the RCS quantities are very low on the decibel scale.

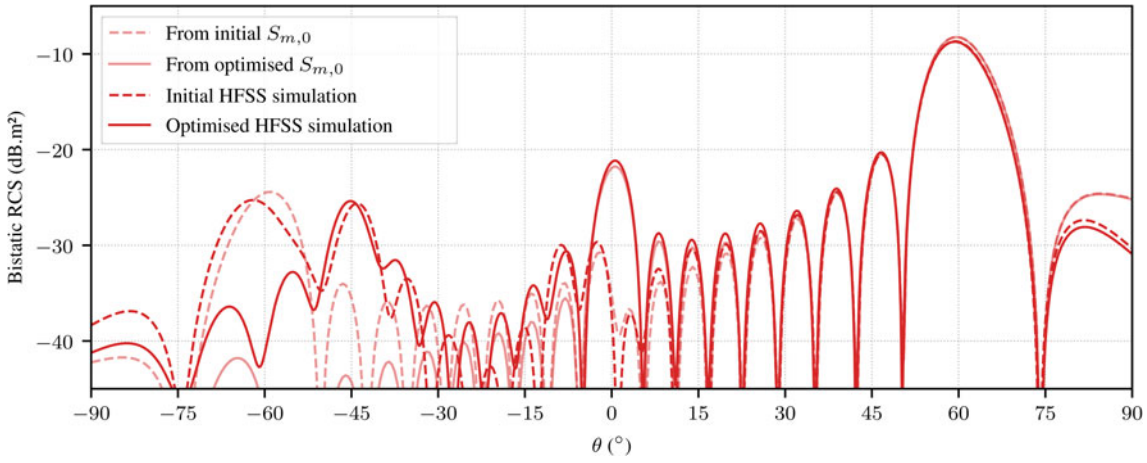


Fig. 9. Bistatic RCS for $\theta_i = 0°$ of the optimized surface compared to the one of the initial surface, in rigorous simulation and by using S parameters. Case $l = 8$ mm.

https://doi.org/10.1017/S1759078722001398 Published online by Cambridge University Press

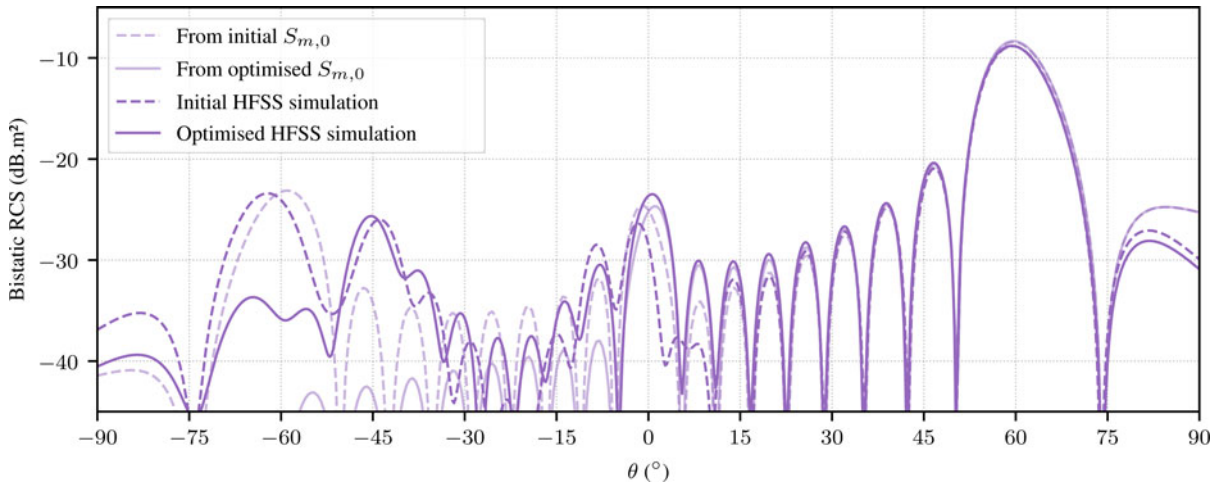


Fig. 10. Bistatic RCS for $\theta_i = 0°$ of the optimized surface compared to the one of the initial surface, in rigorous simulation and by using S parameters. Case $l = 12$ mm.

Table 7. Evolution of the supercell dimensions during the optimization process

p	l_p (mm)	L_p (mm)	φ_p (°)
Initial supercell			
1	12	4.78	120
2	12	5.05	0
3	12	5.17	120
Optimized supercell			
1	11.942	4.828	116.66
2	12.027	5.05	−16.02
3	12.052	5.119	−101.62

Case $l = 12$ mm.

Table 8. Evolution of the supercell $S_{m,0}$ parameters during the optimization process

m	$S_{m,0}$	$\lvert S_{m,0}\rvert$ (dB)
Initial supercell		
−1	$-0.116 - 0.129j$	−15.24
0	$-0.060 + 0.086j$	−19.58
1	$0.948 - 0.032j$	−0.46
Optimized supercell		
−1	$-0.002 - 0.004j$	−46.73
0	$0.059 - 0.085j$	−19.7
1	$0.958 - 0.023j$	−0.37

Case $l = 12$ mm.

Case of l = 12 *mm*

In the same way, concluding results for another case where the starting l value for optimization is 12 mm can be found in Tables 7 and 8 and in Fig. 10.

The $|S_{-1,0}|$ value drops by a great amount as well and the expected RCS diagram shows very low lobe levels for the $\theta = -60°$ direction. Even if the bistatic RCS diagram shows a 10 dB reduction performance in the $\theta = -60°$ direction, the model is less accurate in this angular region, where RCS values are lower. Cell geometry variations are even smaller in this case, actually going under manufacturing precision. Still corroborating the viability of the used technique, this last example could however be unrealistic for practical implementation.

Global results commentary

The three pairs of presented structures exhibit a radiation peak around the −45° area. They also share a lot of their properties, such as array lengths, substrate thickness, cells, and patch shapes for example. It surely goes beyond the scope of the model presented in this publication, but exploring the shared properties of the surfaces should lead to discriminate the origin of this particular radiation.

All the presented structures use the same patch geometry and same degrees of freedom for optimization, but converge to different optimal values. This obviously proves that at least two of them are not global optimums. This is not a surprising conclusion since they all use an initial guess from which it is intended to not deviate too much. This is a way to keep the computing resources needed for optimization very low.

Figure 11 compares phase variations of the cells used in the three initial cases, with respect to L. Globally, the absolute value of the slope at resonance grows as l increases. This gives an explanation about the smaller geometrical variations observed through the three cases, as l is larger for each case.

The case for which $l = 3$ mm shows a smoothly varying phase response with L, but the phase range being in greater L region the resulting cells are wider and then closer to their neighbor in array environment. This could expose them more to coupling effects. In a complementary way, the case for which $l = 12$ mm shows really sensitive phase response regarding L but giving huddled and then isolated cells once in an array. The Floquet-type simulation takes into account the coupling effects between cells in a supercell and between supercells in infinite array. Nevertheless, we may expect slight deviations in the case of a realistic finite array as we have here. The case for which $l = 8$ mm then results in a good trade-off for supercell stability. It is actually the case where the optimized array shows the best performance in attenuating the level of the $S_{-1,0}$ corresponding lobe.

https://doi.org/10.1017/S1759078722001398 Published online by Cambridge University Press

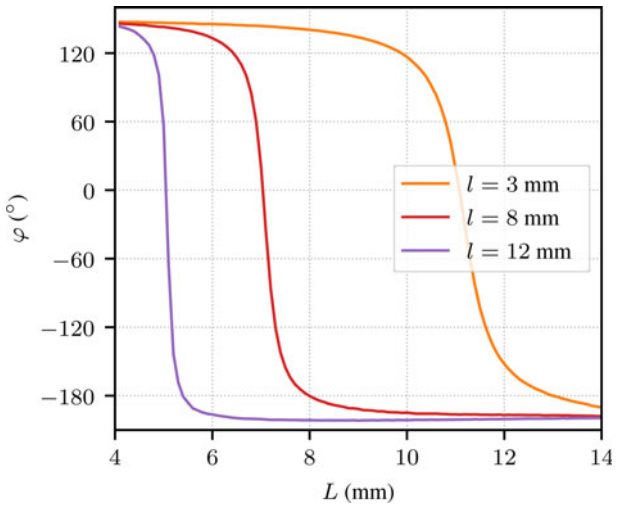


Fig. 11. Phase response, in infinite periodic environment, of the H-shaped patch cells versus L for the three studied cases.

Finally, applying the process to several cases showed the robustness of the proposed method while giving some synthesis advices for this kind of structures.

Conclusion

In this publication we proposed a method that takes advantage of translation invariance usually found in metasurfaces, by using results of Floquet analysis and simulation. After showing the limitations of the classical approach we chose to exploit $S_{m,n}$ simulation parameters to better represent the physical behavior of the structure. After being incorporated in an analytical model, these parameters were manipulated in an optimization process. One first optimization process proved the efficiency of the method and two other cases showed that the method is repeatable, and quantitative with respect to the predicted RCS levels, especially in regions with large RCS returns. In all cases, the proposed optimization method drastically reduced the targeted parasitic radiation. The last discussions also raised some advices, limitations, and tracks for the synthesis of this kind of structure. As the method was tested in simulation environments, future work will focus on experimental validations. In particular, the predicted RCS gains will be verified in the context of a practical implementation with limited manufacturing precision.

Acknowledgements. This work is funded by the French organizations Commissariat á l'Énergie Atomique (CEA) and Agence Innovation Défense (AID).

Conflict of interest. None.

References

1. **M Elineau, R Loison, S Méric, R Gillard, P Pagani, G Mazé-Merceur and P Pouliguen** (2021) Multimode scattering matrix optimisation for the mitigation of harmonics in anomalous reflection metasurfaces. In *51st European Microwave Conference (EuMC),* EuMA, London.
2. **SA Tretyakov** (2015) Metasurfaces for general transformations of electromagnetic fields, Philosophical Transactions of the Royal Society A: mathematical. *Physical and Engineering Sciences* **373**, 0362.
3. **SB Glybovski, SA Tretyakov, PA Belov, YS Kivshar and CR Simovski** (2016) Metasurfaces: from microwaves to visible. *Physics Reports* **634**, 1–27.
4. **R Cacocciola, B Ratni, N Mielec, E Mimoun and S Burokur** (2021) Metasurface-tuning: a camouflaging technique for dielectric obstacles. *Journal of Applied Physics* **129**, 124902.
5. **J Su, H Yu, H Yin, Q Guo, Z Xiao and Z Li** (2021) Breaking the high-frequency limit and bandwidth expansion for radar cross-section reduction: a low-observable technology. *IEEE Antennas and Propagation Magazine* **63**, 75–86.
6. **H Srour, R Gillard, S Méric and D Seetharamdoo** (2018) Analysis of the retrodirective mechanism of a flattened dihedral. *IET Microwaves, Antennas and Propagation* **12**, 0491.
7. **C Yepes, M Faenzi, S Maci and E Martini** (2021) Perfect non-specular reflection with polarization control by using a locally passive metasurface sheet on a grounded dielectric slab. *Applied Physics Letters* **118**, 231601.
8. **A Díaz-Rubio, VS Asadchy, A Elsakka and SA Tretyakov** (2017) From the generalized reflection law to the realization of perfect anomalous reflectors. *Science Advances* **3**, 1602714.
9. **N Yu, P Genevet, MA Kats, F Aieta, J-P Tetienne, F Capasso and Z Gaburro** (2011) Light propagation with phase discontinuities: generalized laws of reflection and refraction. *Science* **334**, 1210713.
10. **S Yin, E Galiffi and A Alù** (2022) Floquet metamaterials. *eLight* **2**, 8.
11. **O Quevedo-Teruel, Q Chen, F Mesa, NJG Fonseca and G Valerio** (2021) On the benefits of glide symmetries for microwave devices. *IEEE Journal of Microwaves* **1**, 457–469.
12. **V Popov, T Lepetit, F Boust and S Burokur** (2021) Sparse metasurfaces: from theory to practical implementations. In *15th European Conference on Antennas and Propagation (EuCAP),* IEEE, New Jersey.
13. **Y Ra'Di, DL Sounas and A Alù** (2017) Metagratings: beyond the limits of graded metasurfaces for wave front control. *Physical Review Letters* **119**, 067404.
14. **VS Asadchy, M Albooyeh, SN Tcvetkova, A Díaz-Rubio, Y Ra'Di and SA Tretyakov** (2016) Perfect control of reflection and refraction using spatially dispersive metasurfaces. *Physical Review B* **94**, 075142.
15. **D Kwon and SA Tretyakov** (2017) Perfect reflection control for impenetrable surfaces using surface waves of orthogonal polarization. *Physical Review B* **96**, 085438.
16. **A Díaz-Rubio and SA Tretyakov** (2021) Macroscopic modeling of anomalously reflecting metasurfaces: angular response and far-field scattering. *IEEE Transactions on Antennas and Propagation* **69**, 6560–6571.
17. **H Haddad, R Loison, R Gillard, A Harmouch and A Jrad** (2019) Mitigation of parasitic reflections over periodic surface impedance modulated panels. In *13th European Conference on Antennas and Propagation (EuCAP),* IEEE, New Jersey.
18. **EF Knott, JF Shaeffer and MT Tuley** (2004) *Introduction, Basic Definitions in Radar Cross Section*. North Carolina: Scitech Publishing, pp. 13–20.
19. **CA Balanis** (2015) *Aperture Antennas in Antenna Theory: Analysis and Design*. New Jersey: John Wiley & Sons, pp. 639–667.
20. **AK Bhattacharyya** (2006) *Introduction to Floquet Modes in Infinite Arrays in Phased Array Antennas*. New Jersey: John Wiley & Sons, pp. 61–83.



Matthieu Elineau is currently pursuing Ph.D. at the National Institute of Applied Sciences (INSA) of Rennes, France. His research activities with the Institut d'Électronique et des Technologies du numérique (IETR; Rennes, France) and the CEA (Le Barp, France) are on the use of metasurfaces for radar applications.



Renaud Loison is a professor at the National Institute of Applied Sciences (INSA), Rennes, France. He carries out his research activity at the Institut d'Électronique et des Technologies du numérique (IETR) and works on reflectarrays, metasurfaces, and more generally on periodic and quasi-periodic surfaces.

https://doi.org/10.1017/S1759078722001398 Published online by Cambridge University Press



Stéphane Méric (M'08) simultaneously graduated in 1991 from the National Institute of Applied Sciences (INSA), Rennes, France, with an electrical engineer diploma and from the University of Rennes 1, with an M.S. in signal processing and telecommunications. He obtained Ph.D. (1996) in electronics from INSA and Habilitation á Diriger des Recherches (HDR) from the University of Rennes 1 in 2016. Since 2000, he is an assistant professor at INSA, and in 2005, he joined the SAPHIR team (IETR–CNRS UMR 6164, Rennes). He was interested in using SAR data in radargrammetric applications. Furthermore, he is currently working on radar system (CW, FMCW) dedicated to specific SAR applications (radar imaging in motorway context, remote sensing, MIMO configuration, and passive radar imaging) and remote-sensing applications. His education activities are about analog electronics, signal processing, radar and radar imaging, and electromagnetic diffraction.



Raphaël Gillard obtained Ph.D. in 1992. He first worked as a research engineer in a company, developing full-wave simulators for microwave circuits and antennas. He joined the National Institute of Applied Sciences (INSA), Rennes, France, in 1993. Since 2001, he has been a full professor with the INSA. His main research interests are computational electromagnetics, reflectarrays, array antennas, dielectric resonator antennas, and periodic structures.



Pascal Pagani obtained M.Sc. in communication systems and signal processing from the University of Bristol, UK, in 2002, Ph.D. in electronics from the National Institute of Applied Sciences (INSA), Rennes, France, in 2005, and habilitation degree from the Université de Bretagne Occidentale, Brest, France in 2016. From 2002 to 2012, he conducted research with Orange Labs in the fields of in-home high data rate communications. He was a recipient of the Grand Prix Général Ferrié in 2013 for his research on transmission over power lines. From 2012 to 2016, he was an associate professor at the graduate engineering school Telecom Bretagne, Brest, France, where he worked on long-haul radio wave propagation and advanced wireline communications. He is currently with the Commissariat á l'Energie Atomique, Le Barp, France, where he specializes in the field of wave-matter interaction in the context of radar, in particular for RCS characterization and reduction.



Geneviève Mazé-Merceur obtained Dipl. Eng., D.E.A., and Ph.D. from École Nationale Supérieure d'Électronique et de Radioélectricité de Grenoble, France, in 1988, 1988, and 1991, respectively. She received Habilitation á Diriger des Recherches from Université de Savoie, France, in 1999. Since 1991, she has been with the Commissariat á l'Énergie Atomique, Le Barp, France. Her research interests include the modeling of electromagnetic wave problems, microwave characterization of materials, and radar cross-section measurements.



Philippe Pouliguen obtained M.S. in signal processing and telecommunications, Ph.D. in electronics, and Habilitation á Diriger des Recherchesé from the University of Rennes 1, Rennes, France, in 1986, 1990, and 2000, respectively. In 1990, he joined the Direction Générale de l'Armement (DGA), DGA Information Superiority (DGA/IS), Bruz, France, where he was a senior expert in electromagnetic radiation and radar signatures. He was also in charge of the Expertise and ElectoMagnetism Computation (EMC) Laboratory, DGA/IS. From 2009 to 2018, he was the head of the "acoustic and radio-electric waves" scientific domain at DGA, Paris, France. Since 2018, he has been the innovation manager of the "acoustic and radio-electric waves" domain at the Agence Innovation Défense (AID), Paris. His research interests include electromagnetic scattering and diffraction, radar cross-section (RCS) measurement and modeling, asymptotic high-frequency methods, radar signal processing and analysis, antenna scattering problems, and electronic bandgap materials.

https://doi.org/10.1017/S1759078722001398 Published online by Cambridge University Press